

Midfield Wireless Powering for Implantable Systems

By JOHN S. HO, *Student Member IEEE*, SANGHOEK KIM, *Student Member IEEE*, AND ADA S. Y. POON, *Senior Member IEEE*

ABSTRACT | Efficient wireless power transfer across tissue is highly desirable for removing bulky energy storage components. Most existing power transfer systems are conceptually based on coils linked by slowly varying magnetic fields (less than 10 MHz). These systems have many important capabilities, but are poorly suited for tiny, millimeter-scale implants where extreme asymmetry between the source and the receiver results in weak coupling. This paper first surveys the analysis of near-field power transfer and associated strategies to optimize efficiency. It then reviews analytical models that show that significantly higher efficiencies can be obtained in the electromagnetic midfield. The performance limits of such systems are explored through optimization of the source, and a numerical example of a cardiac implant demonstrates that millimeter-sized devices are feasible.

KEYWORDS | Implantable systems; midfield; wireless power transfer

I. INTRODUCTION

Implantable medical devices such as cochlear implants, pacemakers, and cardiac defibrillators play an increasingly important role in managing a broad range of medical disorders. These devices interface with physiological processes performing sensing, drug delivery, or local stimulation to monitor or influence their progression. In many applications, miniaturization of the device is crucial for effectiveness and patient safety. Smaller devices can access

narrow channels and cavities ubiquitous in the human body, and are associated with lower clinical risk. While recent progress in microfabrication has dramatically reduced the size of electronic and mechanical components, electrochemical energy storage has been much slower to miniaturize. In most existing devices, the battery constitutes the bulk of the implant.

Wireless powering enables removal of the battery altogether. In place of a battery, a receiver on the implant harnesses energy provided by an external source. Although various means of energy transfer have been studied, including optical, ultrasound, or biological sources, wireless powering through radio-frequency (RF) electromagnetic waves is the most established [1]. In this review, we discuss the conventional design of wireless powering systems based on the electromagnetic near field, and compare this to analyses that show that higher efficiency can be obtained in the midfield when the receiver is much smaller than the source.

Power transfer occurs when a source generates magnetic and electric fields \mathbf{H}_1 and \mathbf{E}_1 that induce voltage V_2 at the receiver. Conventionally, most studies consider frequencies below 10 MHz where the powering configuration consists of coils coupled by their magnetic fields. The magnetic field is preferred for power transfer because it does not interact with most biological material. For a time-harmonic field at frequency ω , the basis of power transfer is Faraday's law

$$V_2 = i\omega\mu_0 \int \mathbf{H}_1 \cdot d\mathbf{s}. \quad (1)$$

It can be seen from this expression that greater voltage can be obtained by increasing ω . However, at higher

Manuscript received January 16, 2012; revised August 12, 2012 and February 4, 2013; accepted February 23, 2013.

The authors are with the Electrical Engineering Department, Stanford University, Stanford, CA 94035 USA (e-mail: adapoon@stanford.edu).

Digital Object Identifier: 10.1109/JPROC.2013.2251851

frequencies, the system behavior deviates from quasi-static approximations. Both reactive and radiative modes are significant, and dielectric dispersion, which is negligible at lower frequencies, characterizes tissue absorption; in most cases, relaxation losses greatly exceed both radiative and ohmic wire losses. For these reasons, higher frequencies were not considered in most analyses. The receiver is thus typically restricted to the near field of the source, where the coupling decays as $1/d^3$ from the source coil. Intuitively, the efficiency degrades rapidly apart from a region of strong coupling.

When the implant is much smaller than its distance from the source, the coupling between the coils is weak. Inductively coupled coils operating in this weakly coupled regime are usually very inefficient. Recently, Poon *et al.* showed that much higher efficiency can be obtained in the midfield where power transfer occurs through a combination of inductive and radiative modes [2], [3]. High efficiency can be realized in spite of increased tissue loss; for most tissue types, the optimal frequency is in the low-gigahertz range. With proper system design, millimeter-sized receivers are possible. Applications that emerge on the scale of these systems include distributed probes for mapping cardiac activity, precise neurostimulators that do not require battery replacement, and locomotive delivery systems that navigate the bloodstream.

We present the two-port network as a means of describing wireless powering in Section II. In Section III, we review powering by inductively coupled coils. Section IV considers the optimal frequency for a point source and receiver; the source is generalized in Section V. In Section VI, midfield wireless powering of a cardiac implant is illustrated, using a computational body model.

II. POWER TRANSFER EFFICIENCY

A. Theory

The exchange of energy due to coupling between the source and the receiver can be described by the two-port network. We have the linear equations

$$V_1 = Z_{11}I_1 + Z_{12}I_2 \quad (2)$$

$$V_2 = Z_{21}I_1 + Z_{22}I_2 \quad (3)$$

where V_1 and V_2 are the time-harmonic voltages across the source and receiver ports, I_1 and I_2 are the currents entering the ports, and Z_{nm} are the impedance parameters of the system. It can be shown by reciprocity that $Z_{12} = Z_{21}$. To describe the object driven by the system, the receiver port is terminated by a load impedance Z_L . Since the receiver is passive, we have $I_2 = -V_2/Z_L$.

At each port, $\text{Re}\{VI^*\}/2$ gives the dissipated power. The real part of the impedance parameters accounts for

loss in the system. Denoting $Z_{nm} = R_n + iX_n$ and $Z_{21} = R_{21} + iX_{21}$, the power transfer efficiency¹ is given by

$$\eta = \frac{R_L |I_2|^2}{R_1 |I_1|^2 + (R_2 + R_L) |I_2|^2 + 2R_{21} \text{Re}\{I_1^* I_2\}} \quad (4)$$

where $I_2/I_1 = -Z_{21}/(Z_{22} + Z_L)$. The efficiency in (4) can be maximized with respect to load impedance Z_L . It can be shown that the optimal load reactance is given by

$$X_{L,\text{opt}} = -X_2 \left(1 - \frac{X_{21}R_{21}}{X_2R_1} \right). \quad (5)$$

For both the strongly and weakly coupled regimes, we will find that $X_{L,\text{opt}} \approx -X_2$ such that the load resonates with receiver. On substituting this approximation into (4), we find that the efficiency is maximized when

$$R_{L,\text{opt}} = R_2 \sqrt{1 - \frac{\text{Re}\{Z_{21}^2\}}{R_1R_2}}. \quad (6)$$

Setting $Z_{L,\text{opt}} = R_{L,\text{opt}} + iX_{L,\text{opt}}$ matches the load impedance to the source such that maximum power transfer occurs. The efficiency η then has the form

$$\eta(Z_{L,\text{opt}}) = \frac{\frac{|Z_{21}|^2}{R_1R_2}}{2 - \frac{\text{Re}\{Z_{21}^2\}}{R_1R_2} + 2\sqrt{1 - \frac{\text{Re}\{Z_{21}^2\}}{R_1R_2}}}. \quad (7)$$

B. Weakly Coupled Regime

When the receiver is small or not in close proximity to the source, wireless powering occurs in the weakly coupled regime where $|Z_{21}|^2/(R_1R_2) \ll 1$. In this regime, the efficiency in (4) can be approximated as

$$\eta \approx \frac{|Z_{21}|^2}{R_1} \frac{R_L}{|Z_{22} + Z_L|^2}. \quad (8)$$

It is easy to show that η is maximized when $Z_{L,\text{opt}} = R_2 - iX_2 = Z_{22}^*$: This is known as conjugate matching. We now define the coupling efficiency

$$\eta_c = \eta(Z_{L,\text{opt}}) = \frac{|Z_{21}|^2}{4R_1R_2} \quad (9)$$

¹This definition for efficiency is also known as the operating power gain. The reflection at the source is disregarded.

which is the ratio of the power available at the receiver to the input power. When the conjugate match condition is satisfied, we have $\eta = \eta_c$; otherwise, it is reduced by a factor

$$\eta_m = \frac{4R_2R_L}{|Z_{22} + Z_L|^2} \quad (10)$$

where in general $\eta = \eta_c\eta_m$. The factor η_m is the matching efficiency and gives the ratio of the power delivered to the load to the available power.

III. INDUCTIVE COUPLING

Inductive coupling has been extensively studied for wireless powering of medical implants, beginning in the 1960s where Schuder *et al.* first demonstrated transfer across the chest wall of animals [4]. There have since been several comprehensive analyses of the inductive link over tissue [5]–[8]. Table 1 lists the parameters of inductively coupled systems described in literature. The list is not exhaustive, but is representative of near-field systems.

The characteristic assumption of inductive coupling is that the fields are slowly changing. For sufficiently low frequencies, the displacement current term of Maxwell’s equations can be ignored; this is known as the quasi-static approximation. The magnetic field under this approximation is distributed around the source. Solutions to this problem are given by either the Biot–Savart law or solving the diffusion equation. Field \mathbf{H}_1 is mostly reactive. From (1), it can be shown that

$$V_2 = -i\omega MI_1 + (i\omega L_2 + R_2)I_2 \quad (11)$$

where M is the mutual inductance. L_n is the self-inductance, and R_n is the lumped resistance of the source and receive coils. Coupling coefficient k is defined as

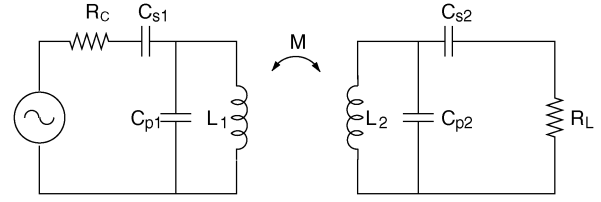


Fig. 1. Lumped circuit model for inductive coupling. The coils can be shunt tuned by inserting capacitors C_{p1} and C_{p2} in parallel or series tuned with C_{s1} and C_{s2} .

$k = M/\sqrt{L_1L_2}$. Since tissue loss is negligible at low frequencies, the parameters are dependent only on the properties of the coils.

The two-port network parameters can be immediately obtained from (11). We have $Z_{12} = Z_{21} = -i\omega M$ and $Z_{nn} = R_n + i\omega L_n$, where R_n is the lumped resistance of the source and receiver coils. A consequence of the quasi-static approximation is that Z_{21} is purely imaginary such that the source and receiver voltage amplitudes are in phase. We find that the optimal load in (5) and (6) simplifies to

$$Z_{L,opt} = R_2 \sqrt{1 - \frac{\text{Re}\{Z_{21}^2\}}{R_1R_2}} - iX_2. \quad (12)$$

In order to obtain high efficiency in (7), it is desirable to operate in the strongly coupled regime $|Z_{21}|^2/R_1R_2 \gg 1$. When coupling Z_{21} is weak, high efficiency can be maintained by reducing the ohmic losses in the coils. The quality factor feasible on implants, however, is typically very limited (< 10) [9].

The optimal load impedance given in (12) is realized by introducing an impedance matching circuit between the receive coil and the load. Since coils are inductive in nature, resonance can be obtained by inserting a capacitor to form an LC tank [an LC tank circuit consists of an inductor (L) and a capacitor (C), and acts as a resonator at a particular frequency], as shown in Fig. 1. Table 2 lists the different tuning configurations that have been studied. Inductance tapping and voltage doubler circuits have also been considered for impedance matching [6]. Coupling can also be enhanced by ferrite cores [24] or efficient rectifying circuits [25].

Table 1 Frequency, Range, and Coil Size of Select Implants

Implant Type	Carrier (MHz)	Range	Source Coil	Receiver Coil
Generic [10]	1-2	0.5 cm	1 cm	0.47 cm
Generic [11]	4	0.8 cm		
Generic [12]	10	1.5 cm	3.5 cm	2.7 cm
Cortical visual [13]	5,10,33	1 cm		
Retinal [14]	1-10			
Retinal [15]	2.5	0.575 cm	1.34 cm	1.34 cm
Muscular [16], [17]	2		9-20 cm	0.12 cm
Muscular [18]	6.78			
Muscular [19]	2			
Bio-sensor [20]	27	9 cm		5 cm
Sensor [21]	0.133	< 1 m		
Sensor [22]	13.56	10 cm	15 cm	6 cm
Sensor [23]	3.18	4 cm	4.8 cm	0.6 cm

Table 2 Tuning Configurations of Select Studies

Reference	Transmit Tuning	Receive Tuning	Resonance
[26]	–	shunt	unloaded
[27]	series	shunt	loaded
[28]	shunt	shunt	unloaded
[7], [29]	stagger	stagger	–
[30]–[33]	series	series	–
[34]	series-shunt	shunt	–

Many techniques to improve the robustness of the link have also been studied. In [26], displacement tolerance was improved with a small degradation in efficiency from the untuned counterpart. In [27], the dependency of the efficiency on coupling coefficient k was reduced by operating at the optimal voltage transfer ratio. A similar idea was proposed in [28], where k maximized transimpedance to desensitize its variation with k . In [7] and [29], the voltage transfer ratio was desensitized to variation in k by staggered tuning circuits. Using coils at free-running oscillation, it was shown that the efficiency is independent of coupling if k is greater than the inverse of the loaded quality factor of the receive coil [30]–[33]. In [34], a circuit approach was described to improve the tolerance to coupling variation using coils at self oscillation. In most of these techniques, the idea of using resonant LC tanks on both coils to enhance the efficiency is deeply embedded. Recent studies on midrange power transfer in air are reminiscent of this idea [35], [36].

IV. HIGHER FREQUENCIES

When the source–receiver separation is on the order of a wavelength from the source, the powering system operates in the midfield. This corresponds to frequencies in the low-gigahertz range at typical distances of separation. Here, the general system behavior deviates from quasi-static approximations. The fields are characterized by a combination of reactive and radiative modes. In [2] and [3], it was shown that when the source and the receiver are weakly coupled, optimal power transfer occurs in the midfield. The analyses considered millimeter-sized source and receiver coils in a homogenous tissue environment. The coils are spaced several centimeters apart such that $|Z_{21}|^2/R_{11}R_{22} \ll 1$ across all frequencies of interest.

A. Two-Port Network Parameters

The impedance parameters of the system can be obtained by power arguments. In particular, it can be shown that $|Z_{21}|^2/R_1R_2 = |V_{oc}|^2/2P_1R_2$ where V_{oc} is the open-circuit voltage induced at the receive coil and P_1 is the power loss due to R_1 . Here, P_1 is equal to the sum of losses in the source, which include radiative, resistive, and tissue losses. Characterizing only tissue loss

$$R_1 = \frac{\omega}{|I_1|^2} \int \text{Im}\epsilon(\mathbf{r}) |\mathbf{E}_1(\mathbf{r})|^2 d\mathbf{r}. \quad (13)$$

Parameter R_2 can be obtained in the same manner. By examining the induced voltage in the receive coil, it can also be shown that

$$Z_{21} = \frac{1}{I_1 I_2} \int \mathbf{M}_2(\mathbf{r}) \cdot \mathbf{H}_1(\mathbf{r}) d\mathbf{r} \quad (14)$$

where \mathbf{M}_2 is the magnetic current density due to the dipole moment generated by the receive coil. In contrast to the near field, the real part of Z_{21} is generally nonzero so the voltage amplitudes at the source and the receiver may not be in phase.

Fields \mathbf{H}_1 and \mathbf{E}_1 can be expressed in terms of a source magnetic current density \mathbf{M}_1

$$\mathbf{H}_1(\mathbf{r}) = i\omega\epsilon(\mathbf{r}) \int \bar{\mathbf{G}}_H(\mathbf{r}, \mathbf{r}') \mathbf{M}_1(\mathbf{r}') d\mathbf{r}' \quad (15)$$

$$\mathbf{E}_1(\mathbf{r}) = - \int \bar{\mathbf{G}}_E(\mathbf{r}, \mathbf{r}') \mathbf{M}_1(\mathbf{r}') d\mathbf{r}' \quad (16)$$

where $\bar{\mathbf{G}}_H$ and $\bar{\mathbf{G}}_E$ are the dyadic Green's functions for a magnetic current source. They have a simple analytical form for homogeneous tissue and can be understood as the fields generated by a point source.

B. Optimal Frequency

The optimal ω is defined to be the frequency where efficiency is maximized independent of coil or matching considerations. Referring to (8), we see that this corresponds to maximization of the coupling parameter $\gamma = |Z_{21}|^2/R_1$. For a coil of area A_r oriented in direction $\hat{\mathbf{n}}$, the magnetic dipole moment can be approximated by $\mathbf{M} = i\omega\mu_0 A_r I \delta(\mathbf{r} - \mathbf{r}_0) \hat{\mathbf{n}}$. The coupling parameter is then given by

$$\gamma = \frac{|V_{oc}|^2}{2P_1} = \frac{\omega\mu_0^2 A_r^2 |\mathbf{H}_1(\mathbf{r}_f) \cdot \hat{\mathbf{n}}|^2}{\int \text{Im}\epsilon(\mathbf{r}) |\mathbf{E}_1(\mathbf{r})|^2 d\mathbf{r}}. \quad (17)$$

It can be seen from this expression that as ω increases, induced voltage V_{oc} also increases; this gain, however, is eventually offset by dielectric losses.

Tissue is taken into account by modeling the two mechanisms of tissue loss: tissue conductivity and dielectric relaxation. The Debye relaxation model is widely used for biological media and describes both phenomena by the parameter

$$\epsilon_r(\omega) = \epsilon_\infty + \frac{\epsilon_{r0} - \epsilon_\infty}{1 - i\omega\tau} + i \frac{\sigma}{\omega\epsilon_0} \quad (18)$$

where ϵ_r is the dielectric permittivity of tissue. Parameters ϵ_{r0} , ϵ_∞ , σ , and τ are given in [37] for different types of tissue.

In [2], face-to-face (0°) and edge-to-edge (90°) orientations for the coils were considered. Bounds for the optimal frequency were then obtained using asymptotic expressions for the dielectric permittivity. A more accurate approximation can be obtained by decomposing Green's

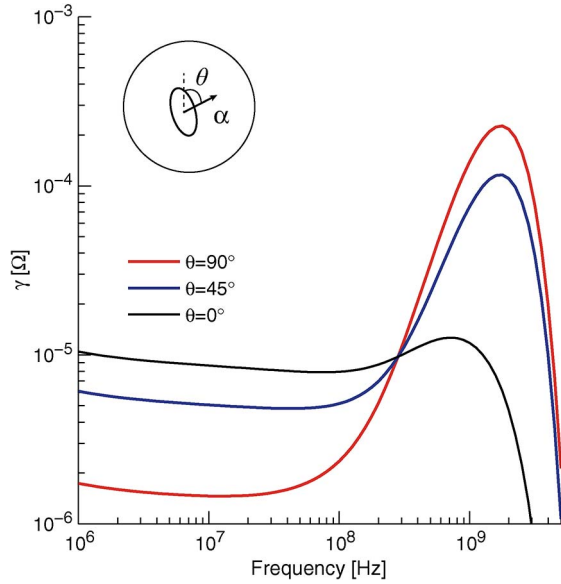


Fig. 2. Coupling parameter γ versus frequency for two identical coils with dipole moments α in direction θ . The coils are in muscle and positioned 5 cm apart.

functions into the sum of vector multipoles [38]. Considering only the lowest order multipoles [3], the optimal frequency was shown to be approximately

$$f_{\text{opt}} \approx \frac{1}{2\pi} \sqrt{\frac{c\sqrt{\epsilon_{r0}}}{\tau d(\epsilon_{r0} - \epsilon_{\infty})}} \quad (19)$$

where d is the distance between the source and the receiver.

As a numerical example, we consider coils with area $A_r = 4 \text{ mm}^2$ in muscle tissue. Fig. 2 shows γ over a range of frequencies for the face-to-face, 45° tilt, and edge-to-edge orientations. At frequencies around 10 MHz, high efficiency is obtained at the $\theta = 0^\circ$ orientation. This effect can be attributed to the fact that, in the near field, the dominant magnetic field component lies in the direction of the dipole moment. In the midfield, however, the transverse component is dominant since the optimal orientation is $\theta = 90^\circ$. Unlike in the far field, however, the magnetic field component in the direction of propagation is still significant. For all orientations, the optimal frequency occurs in the low-gigahertz range.

The approximate optimal frequencies in (19) are listed in Table 3 for different tissues. Other practical reasons exist for operating at higher frequencies. The received open-circuit voltage increases linearly with frequency; potentials exceeding the threshold voltage of typical transistors are required to start up the power harvesting circuitry [39]. If data are modulated onto the power carrier, in-

Table 3 Approximate Optimal Frequency at 5-cm Depth for Select Types of Human Tissue

Tissue Type	Approximate f_{opt} (GHz)
Blood	1.58
Bone (cancellous)	1.70
Bone (cortical)	2.01
Fat (infiltrated)	2.68
Fat (not infiltrated)	3.86
Heart	1.68
Liver	1.70
Lung (deinflated)	1.72
Muscle	1.76
Skin (dry)	1.98
Skin (wet)	1.79

creasing the operating frequency also enables higher data rates [40].

V. GENERAL SOURCE

Near-field power transfer systems typically consist of source and receiver structures based on coil structures. The characteristics of power transfer do not change significantly with alternative designs because, at distances less than a wavelength, the fields are insensitive to the precise shape of the source. Beyond the near field, however, the field patterns are determined by the interference of radiation from the distribution of sources. Efficiency can be enhanced by concentrating radiation, a property often exploited by antennas and antenna arrays, but the performance is fundamentally limited by the physics of wave propagation in tissue. In this section, we review an analytical solution for the optimal source and the derived characteristics that enable efficient power transfer to tiny devices.

Kim *et al.* studied wireless powering with the general configuration in Fig. 3(a) [41], [42]. The system consists of a source positioned over a small receiving coil embedded in tissue. The tissue is approximated by dielectric multilayers: the simple geometry permits analytical treatment while retaining the essential features, such as the behavior of waves at tissue interfaces, of the problem. Formally, a source is described by its 3-D electric current density. Direct optimization over the space of such sources, however, generally involves intractable complexities. Here, using a representation based on the field equivalence principle, the source is restricted to an in-plane electric current density \mathbf{J}_1 . It can be shown that every source has a representation in this form: given an arbitrary, 3-D source of radiation, there exists a \mathbf{J}_1 that generates the same electromagnetic fields. The current density that is optimal in this parameter space, therefore, bounds performance that can be obtained by any physical realization of the source.

We now isolate the parameters in the efficiency expression (8) that involve source fields. It can be seen that parameter $\gamma = |Z_{21}|^2/R_1$ used in Section IV also characterizes

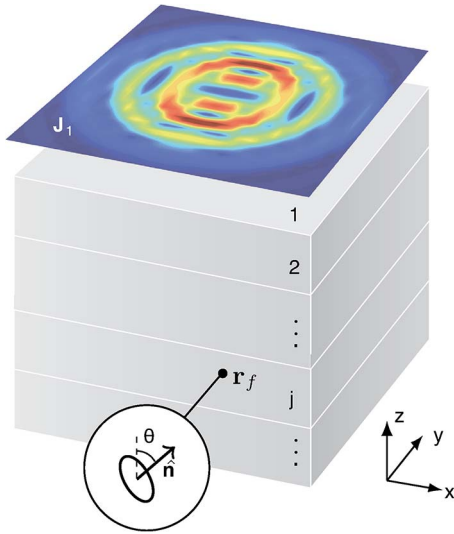


Fig. 3. The multilayer tissue model consists of n stacked layers, each with dielectric permittivity ϵ_{ij} , and the receiver is placed at depth z_f in the layers. The source consists of an electric current density \mathbf{J}_1 tangential to the $z = 0$ plane. It can be shown from the equivalence principle that for every source located in the $z > 0$ half-space, there exists a \mathbf{J}_1 that generates identical fields in the $z < 0$ half-space.

dependence on the source. Optimal power transfer thus occurs for the particular choice of source \mathbf{J}_1 that generates electromagnetic fields maximizing γ as given in (17). The fields in this expression are again given by the integral equations $\mathbf{E}_1(\mathbf{r}) = i\omega\mu \int \bar{\mathbf{G}}_E(\mathbf{r} - \mathbf{r}')\mathbf{J}_1(\mathbf{r}')d\mathbf{r}'$ and $\mathbf{H}_1(\mathbf{r}) = \int \bar{\mathbf{G}}_H(\mathbf{r} - \mathbf{r}')\mathbf{J}_1(\mathbf{r}')d\mathbf{r}'$, where Green's functions for the electric current are suitably modified for the tissue geometry.

For a multilayer structure, the angular decomposition of Green's functions has a simple form based on the propagation of the component plane waves in terms of reflection and transmission coefficients. Applying a Fourier transform in each of the lateral coordinates x and y , the integral equations are reduced to multiplication with a propagation matrix. We find that γ can be written as

$$\gamma = \frac{\omega\mu_0^2 A_r^2 \left| \int \bar{\mathbf{G}}_H(z_f)\hat{\mathbf{n}} \cdot \mathcal{J}_1 d\mathbf{k}_s \right|^2}{4\pi^2 \int \mathcal{J}_1^* \left(\int \text{Im}\epsilon \bar{\mathbf{G}}_E^*(z)\bar{\mathbf{G}}_E(z) dz \right) \mathcal{J}_1 d\mathbf{k}_s} \quad (20)$$

where transform variable \mathbf{k}_s has been suppressed for notional simplicity. Here, γ is in a form such that maximization with respect to \mathcal{J}_1 corresponds to the well-known matched filter problem [43]. An upper bound to the ratio (20) can be established through the Cauchy–Schwarz inequality, from which it can be shown that equality holds when

$$\mathcal{J}_{\text{opt}} = \left(\int \text{Im}\epsilon \bar{\mathbf{G}}_E^*(z)\bar{\mathbf{G}}_E(z) dz \right)^{-1} \bar{\mathbf{G}}_H^*(z_f)\hat{\mathbf{n}}. \quad (21)$$

Table 4 Multilayer Model for the Cardiac Implant

Layer j	Type	Thickness (cm)	d_j (cm)
1	Air	1.0	1.0
2	Skin	0.2	1.2
3	Fat	1.0	2.2
4	Muscle	0.8	3.0
5	Bone	1.6	4.6
6	Heart	∞	–

The optimal current density is recovered by an inverse transform.

As a numerical example, we consider a multilayer tissue structure with composition approximating the chest wall (Table 4) and a receive coil of radius 1 mm positioned 5 cm from the source. We obtain the optimal source from (21) for frequencies ranging from 100 MHz to 5 GHz. Coil-based structures, generated by varying the radius of a perfectly conducting loop from 0.3 to 3 cm, serve as reference sources. Other primitive structures, such as a linear dipole or uniform density, result in large reactive electric fields and, thus, do not yield greater efficiency.

Fig. 4(a) shows that the theoretical bound holds across the entire frequency range. Consistent with the simpler analytical model in Section IV, maximum coupling is obtained in the low-gigahertz range for a receiver oriented 90° . At 2.6 GHz where the peak efficiency occurs, the performance of the optimal source exceeds the best coil-based structure [Fig. 4(b)] by a factor of 5.

The optimal current density, shown in Fig. 4(c), consists of alternating current paths spaced approximately every half wavelength. The current paths propagate inwards, generating fields that exhibit the focusing effect, as shown in Fig. 4(d) and (e). The interference of radiation produces concentrated power flow to the receiver. In contrast, coils operating in the midfield have divergent power flow lines. Although a source of infinite extent is permitted in the formulation, the amplitude of the optimal source tapers with radial distance from the center. This property facilitates practical implementation: optimal power transfer may be closely approximated by sources of compact sizes.

VI. POWER TRANSFER TO A CARDIAC IMPLANT

In [44], Kim *et al.* studied midfield power transfer to a millimeter-sized cardiac implant using an electromagnetic model of the human body [45]. The configuration consists of an external source described by a planar current density, as in Section V, positioned 5 cm above a receive coil on the surface of the heart. The optimal source is solved by computational methods since the complex tissue geometry does not admit analytical treatment.

Source \mathbf{J}_1 was discretized into a 15×15 array of electric dipoles equally spaced 8 mm apart and oriented arbitrarily in the plane. The dimensions were found sufficient

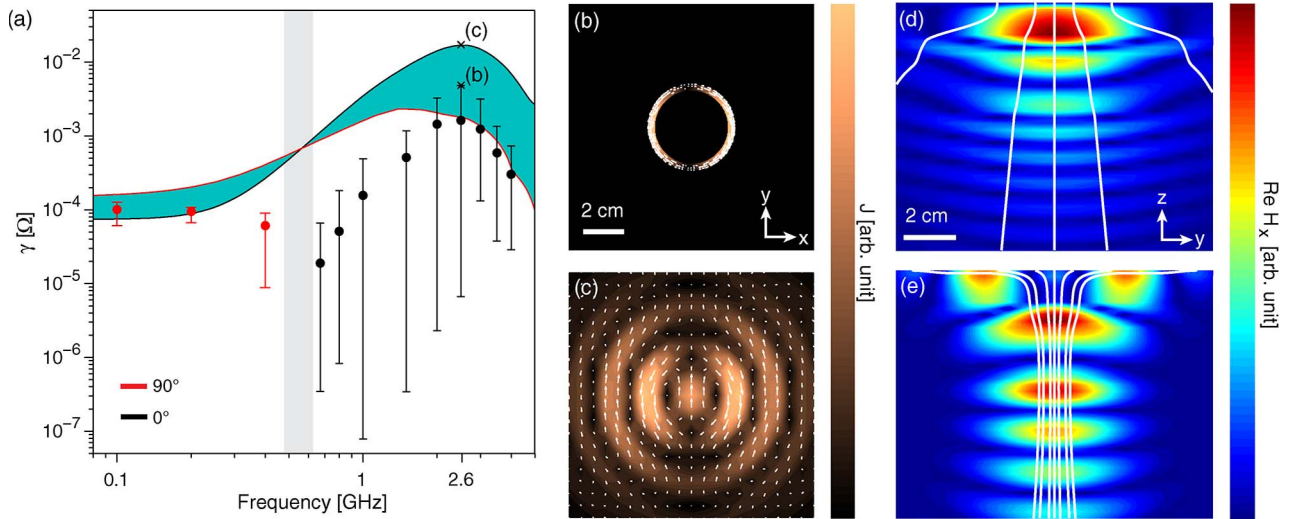


Fig. 4. (a) Theoretical bound on γ for the $\theta = 90^\circ$ (black) and the $\theta = 0^\circ$ (red) receive coil orientations. Coil-based source structures with radii from 0.3 to 3 cm (error bars show the max, min, and mean) achieve efficiencies below the theoretical bound. The near-field to midfield transition region is shaded. (b) and (c) Current distribution of the coil source (top) and the optimal source (bottom) at 2.6 GHz. (d) and (e) The magnetic field component aligned with the receiver dipole moment \hat{x} and the Poynting vector (white) generated by the coil source (top) and the optimal source (bottom) at 2.6 GHz.

to closely approximate the optimal current distribution for the multilayer model. The fields due to each dipole are calculated by the finite-difference time domain (FDTD)

for each component, and the weights maximizing γ can be found by a matrix inversion [46]. R_2 was analytically calculated for a small coil in heart tissue. In addition to FDTD calculation, a theoretical η is also found for the multilayer model approximating the chest in Table 4.

At each frequency ω , the optimal efficiency η was evaluated by the following procedure. First, source \mathbf{J}_1 that maximizes γ was found. Next, R_2 for the receive coil was computed; the coupling efficiency in (9) is given by $\gamma/4R_2$. Finally, the matching efficiency in (10) was determined by

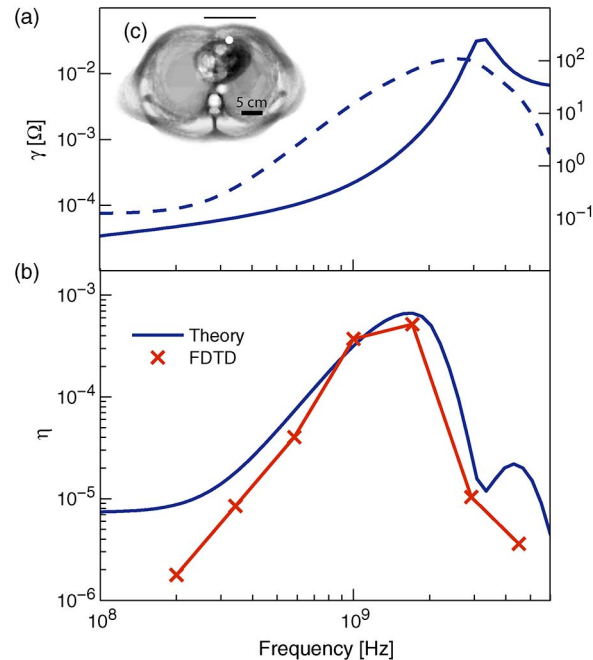


Fig. 5. (a) Theoretical γ (dashed) and R_2 (solid) as a function of frequency computed over the multilayer model. (b) Efficiency η for the theoretical multilayer model and FDTD body model calculation. (c) Receive coil placement on the surface of the heart 5 cm from the external source. The coil is oriented in the 90° direction.

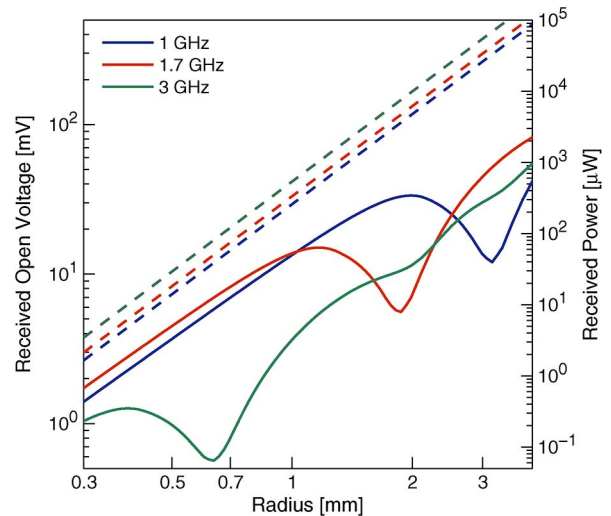


Fig. 6. Open-circuit voltage (dashed) and received power (solid) as a function of the receive coil size.

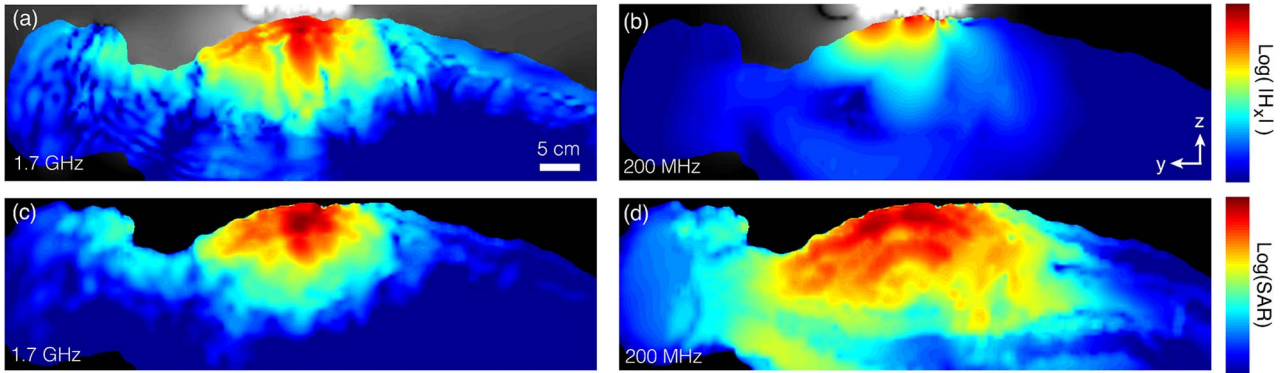


Fig. 7. Midfield and near-field wireless powering comparison for a cardiac implant with a discretized 15×15 optimized source. The log intensity of the magnetic field component aligned with the receiver dipole moment \hat{x} is shown in (a) at 1.7 GHz and (b) at 200 MHz. The absorbed power measured in SAR is shown in (c) at 1.7 GHz and (d) at 200 MHz. All fields have been normalized such that the maximum SAR is the same at both frequencies.

setting R_L as close to R_2 as possible. Perfect matching $R_L = R_2$ is not always possible due to the limited transformation range of matching networks. For quality factors less than 10, the maximum impedance transformation ratio is 1 : 100 [9]. The minimum value of R_L was set to 10 Ω based on a load of the typical impedance 1 k Ω .

Fig. 5(a) and (b) shows the efficiency computed from the theoretical γ and R_2 . The maximum efficiency occurs at 1.7 GHz and is about two orders of magnitude higher than the efficiencies obtained at megahertz frequencies. R_2 exhibits a peak due to the self-resonance of the receiver coil. The FDTD results agree closely with the theoretical calculations around 1 GHz, but deviate below 300 MHz or above 3 GHz, since the source and the body model are no longer well approximated by the multilayer geometry.

Fig. 6 shows the maximum received power and open-circuit voltage under the tissue heating constraint versus the receiver coil size. The received power dips at the R_2 resonant peak. The drop, however, can be avoided by operating at a different frequency. In the midfield, an open-circuit voltage of 47.7 mV and power of 51.2 μ W can be received by a 1-mm coil. The received power is sufficient to operate typical implants: a pacemaker consuming 8 μ W, for example, was reported in [47]. Such millimeter-sized coils are about an order of magnitude smaller than the inductively coupled receivers in Table 1.

Estimates of received power levels can be calculated from these efficiencies by considering the maximum

power at the source. For typical applications, safety guidelines specify that the specific absorption rate (SAR) is not to exceed 1.6 mW/cm³ [48] for general safety. As a convenient reference, the transmit power is normalized such that the peak SAR equals the safety guideline. The received voltage and SAR, normalized to the safety guideline, along a slice of the body model are shown in Fig. 7. Focusing can be seen in the low-gigahertz range, but it is not observed at 200 MHz due to the relatively long wavelength.

VII. CONCLUSION

When the source and the receiver are weakly coupled, midfield wireless powering obtains much higher efficiency than near-field systems. With proper design of the source, millimeter-sized receivers are possible at higher frequencies despite increased tissue loss. Prototypes of implantable devices operating at higher frequencies have recently been demonstrated in literature [39], [40].

In order to realize the efficiencies obtained in analysis, we note that the optimal source current distribution must be synthesized by a physical antenna. The limits derived in midfield analysis, however, show that the theoretical bound on performance far exceeds the efficiencies obtained by conventional designs. The realization of such midfield systems could enable the capabilities of existing medical devices to be replicated at new physiological scales. ■

REFERENCES

- [1] W. Phillips, B. Towe, and P. Larson, "An ultrasonically-driven piezoelectric neural stimulator," in *Proc. 25th Annu. Int. Conf. IEEE Eng. Med. Biol.*, Sep. 2003, vol. 2, pp. 1983–1986.
- [2] A. S. Y. Poon, S. O'Driscoll, and T. H. Meng, "Optimal operating frequency in wireless power transmission for implantable devices," in *Proc. Annu. Int. Conf. IEEE Eng. Med. Biol.*, Lyon, France, Aug. 2007, pp. 5673–5678.
- [3] A. S. Y. Poon, S. O'Driscoll, and T. H. Meng, "Optimal frequency for wireless power transmission over dispersive tissue," *IEEE Trans. Antennas Propag.*, vol. 58, no. 5, pp. 1739–1749, May 2010.
- [4] J. C. Schuder, H. E. Stephenson, Jr., and J. F. Townsend, "High-level electromagnetic energy transfer through a closed chest wall," *IRE Int. Conv. Rec.*, vol. 9, pp. 119–126, 1961.
- [5] F. C. Flack, E. D. James, and D. M. Schlapp, "Mutual inductance of air-cored coils: Effect on design of radio-frequency coupled implants," *Med. Biol. Eng.*, vol. 9, no. 2, pp. 79–85, Mar. 1971.

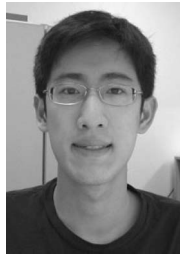
- [6] W. H. Ko, S. P. Liang, and C. D. Fung, "Design of radio-frequency powered coils for implant instruments," *Med. Biol. Eng. Comput.*, vol. 15, pp. 634–640, 1977.
- [7] D. C. Galbraith, "An implantable multichannel neural stimulator," Ph.D. dissertation, Elect. Eng., Stanford Univ., Stanford, CA, USA, Dec. 1984.
- [8] W. J. Heetderks, "RF powering of millimeter- and submillimeter-sized neural prosthetic implants," *IEEE Trans. Biomed. Eng.*, vol. 35, no. 5, pp. 323–327, May 1988.
- [9] T. H. Lee, *The Design of CMOS Radio-Frequency Integrated Circuits*. Cambridge, U.K.: Cambridge Univ. Press, 1998.
- [10] T. Akin, K. Najafi, and R. M. Bradley, "A wireless implantable multichannel digital neural recording system for a micromachined sieve electrode," *IEEE J. Solid-State Circuits*, vol. 33, no. 1, pp. 109–118, Jan. 1998.
- [11] H. Yu and K. Najafi, "Low-power interface circuits for bio-implantable microsystems," in *Proc. Int. IEEE Solid-State Circuits Conf. (ISSCC)*, San Francisco, CA, Feb. 2003, vol. 1, pp. 194–487.
- [12] Y. Hu and M. Sawan, "A fully integrated low-power BPSK demodulator for implantable medical devices," *IEEE Trans. Circuits Syst. I, Reg. Papers*, vol. 52, no. 12, pp. 2552–2562, Dec. 2005.
- [13] M. Piedade, J. Gerald, L. A. Sousa, G. Tavares, and P. Tomas, "Visual neuroprosthesis: A non invasive system for stimulating the cortex," *IEEE Trans. Circuits Syst. I, Reg. Papers*, vol. 52, no. 12, pp. 2648–2662, Dec. 2005.
- [14] W. Liu, K. Vichienchom, M. Clements, S. C. DeMarco, C. Hughes, E. McGuckin, M. S. Humayun, E. de Juan, J. D. Weiland, and R. Greenberg, "A neuro-stimulus chip with telemetry unit for retinal prosthetic device," *IEEE J. Solid-State Circuits*, vol. 35, no. 10, pp. 1487–1497, Oct. 2000.
- [15] G. J. Suaning and N. H. Lovell, "CMOS neurostimulation ASIC with 100 channels, scalable output, and bidirectional radio-frequency telemetry," *IEEE Trans. Biomed. Eng.*, vol. 48, no. 2, pp. 248–260, Feb. 2001.
- [16] T. Cameron, G. E. Loeb, R. A. Peck, J. H. Schulman, P. Strojnik, and P. R. Troyk, "Micromodular implants to provide electrical stimulation of paralyzed muscles and limbs," *IEEE Trans. Biomed. Eng.*, vol. 44, no. 9, pp. 781–790, Sep. 1997.
- [17] G. E. Loeb and R. Davoodi, "The functional reanimation of paralyzed limbs," *IEEE Eng. Med. Biol. Mag.*, vol. 24, no. 5, pp. 45–51, Sep. 2005.
- [18] B. Smith, Z. Tang, M. W. Johnson, S. Pourmehdi, M. M. Gazdik, J. R. Buckett, and P. H. Peckham, "An externally powered, multichannel, implantable stimulator-telemeter for control of paralyzed muscle," *IEEE Trans. Biomed. Eng.*, vol. 45, no. 4, pp. 463–475, Apr. 1998.
- [19] S. Y. Lee and S. C. Lee, "An implantable wireless bidirectional communication microstimulator for neuromuscular stimulation," *IEEE Trans. Circuits Syst. I, Reg. Papers*, vol. 52, no. 12, pp. 2526–2538, Dec. 2005.
- [20] Q. Huang and M. Oberle, "A 0.5-mW passive telemetry IC for biomedical applications," *IEEE J. Solid-State Circuits*, vol. 33, no. 7, pp. 937–946, Jul. 1998.
- [21] T. van den Boom, D. Tebmann, R. Lerch, G. vom Bögel, D. Hammerschmidt, J. Amelung, B. Hosticka, and P. Mahdavi, "Remote CMOS pressure sensor chip with wireless power and data transmission," in *Proc. Int. IEEE Solid-State Circuits Conf.*, San Francisco, CA, Feb. 2000, pp. 186–187.
- [22] O. Chevalerias, T. O'Donnell, D. Power, N. O'Donovan, G. Duffy, G. Grant, and S. C. O'Mathuna, "Inductive telemetry of multiple sensor modules," *IEEE Perv. Comput.*, vol. 4, no. 1, pp. 46–52, Jan. 2005.
- [23] A. D. DeHennis and K. D. Wise, "A wireless microsystem for the remote sensing of pressure, temperature, and relative humidity," *J. Microelectromech. Syst.*, vol. 14, no. 1, pp. 12–22, Feb. 2005.
- [24] J. C. Schuder and H. E. Stephenson, Jr., "Energy transport to a coil which circumscribes a ferrite core and is implanted within the body," *IEEE Trans. Biomed. Eng.*, vol. BME-12, no. 3–4, pp. 154–163, Jul./Oct. 1965.
- [25] R. Kadefors, E. Kaiser, and I. Petersen, "Energizing implantable transmitters by means of coupled inductance coils," *IEEE Trans. Biomed. Eng.*, vol. BME-16, no. 3, pp. 177–183, Jul. 1969.
- [26] I. C. Forster, "Theoretical design and implementation of transcutaneous multichannel stimulator for neural prostheses applications," *J. Biomed. Eng.*, vol. 3, pp. 107–120, Apr. 1981.
- [27] N. de N. Donaldson and T. A. Perkins, "Analysis of resonant coupled coils in the design of radio-frequency transcutaneous links," *Med. Biol. Eng. Comput.*, vol. 21, pp. 612–627, Sep. 1983.
- [28] E. S. Hochmair, "System optimization for improved accuracy in transcutaneous signal and power transmission," *IEEE Trans. Biomed. Eng.*, vol. BME-31, no. 2, pp. 177–186, Feb. 1984.
- [29] D. C. Galbraith, M. Soma, and R. L. White, "A wide-band efficient inductive transdermal power and data link with coupling insensitive gain," *IEEE Trans. Biomed. Eng.*, vol. BME-34, no. 4, pp. 265–275, Apr. 1987.
- [30] P. E. K. Donaldson, "Frequency-hopping in R.F. energy-transfer links," *Electron. Wireless World*, pp. 24–26, Aug. 1986.
- [31] P. E. K. Donaldson, "Three separation-insensitive radiofrequency inductive links," *J. Med. Eng. Technol.*, vol. 11, no. 1, pp. 23–29, Jan. 1987.
- [32] P. E. K. Donaldson, "Power for neurological prostheses: A simple inductive R.F. link with improved performance," *J. Biomed. Eng.*, vol. 9, pp. 194–197, Jun. 1987.
- [33] T. Ivall, "Does your coupling coefficient matter?" *Electron. Wireless World*, vol. 93, no. 6, pp. 577–579, 1987.
- [34] C. M. Zierhofer and E. S. Hochmair, "High-efficiency coupling-insensitive transcutaneous power and data transmission via an inductive link," *IEEE Trans. Biomed. Eng.*, vol. 37, no. 7, pp. 716–722, Jul. 1990.
- [35] A. Kurs, A. Karalis, R. Moffatt, J. D. Joannopoulos, P. Fisher, and M. Soljacic, "Wireless power transfer via strongly coupled magnetic resonances," *Science*, vol. 317, pp. 83–86, Jul. 2007.
- [36] X. Yu, S. Sandhu, S. Beiker, R. Sassoon, and S. Fan, "Wireless energy transfer with the presence of metallic planes," *Appl. Phys. Lett.*, vol. 99, no. 21, 2114102.
- [37] S. Gabriel, R. W. Lau, and C. Gabriel, "The dielectric properties of biological tissues: III. parametric models for the dielectric spectrum of tissues," *Phys. Med. Biol.*, vol. 41, no. 11, pp. 2271–2293, Nov. 1996.
- [38] W. C. Chew, *Waves and Fields in Inhomogeneous Media*. Piscataway, NJ, USA: IEEE Press, 1995.
- [39] S. O'Driscoll, A. S. Y. Poon, and T. H. Meng, "A mm-sized implantable power receiver with adaptive link compensation," in *Proc. IEEE Int. Solid-State Circuits Conf.*, San Francisco, CA, Feb. 2009, pp. 294–295.
- [40] A. Yakovlev, D. Pivonka, T. H. Meng, and A. S. Y. Poon, "A mm-sized wirelessly powered and remotely controlled locomotive implantable device," in *Proc. IEEE Int. Solid-State Circuits Conf.*, San Francisco, CA, Feb. 2012, pp. 302–304.
- [41] S. Kim, J. S. Ho, and A. S. Y. Poon, "Wireless power transfer to miniature implants: Transmitter optimization," *IEEE Trans. Antennas Propag.*, vol. 60, no. 10, pp. 4838–4845, Oct. 2012.
- [42] S. Kim, J. S. Ho, and A. S. Y. Poon, "Source optimization for wireless powering of tiny implants," under review.
- [43] V. Poor, "Robust matched filters," *IEEE Trans. Inf. Theory*, vol. IT-29, no. 5, pp. 677–687, Sep. 1983.
- [44] S. Kim, J. S. Ho, L. Y. Chen, and A. S. Y. Poon, "Wireless power transfer to a cardiac implant," *Appl. Phys. Lett.*, vol. 101, no. 7, 073701.
- [45] G. I. Zubal, "Computerized three-dimensional segmented human anatomy," *Amer. Assoc. Phys. Med.*, vol. 21, no. 2, pp. 299–302, 1993.
- [46] S. Kim and A. S. Y. Poon, "Optimizations of source distribution in wireless power transmission for implantable devices," in *Proc. IEEE Antennas Propag. Symp.*, Toronto, ON, Canada, Jul. 2010, pp. 20–25.
- [47] L. S. Y. Wong, S. Hossain, A. Ta, J. Edvinsson, D. H. Rivas, and H. Naas, "A very low-power CMOS mixed-signal IC for implantable pacemaker applications," *IEEE J. Solid-State Circuits*, vol. 39, no. 12, pp. 2446–2456, Dec. 2004.
- [48] *IEEE Standard for Safety With Respect to Human Exposure to Radiofrequency Electromagnetic Fields, 3 kHz to 300 GHz*, IEEE Standard C95.1-1999, 1999.

Ho et al: Midfield Wireless Powering for Implantable Systems

ABOUT THE AUTHORS

John S. Ho (Student Member, IEEE) was born in California. He received the B.Eng degree in electronic and computer engineering from Hong Kong University of Science and Technology (HKUST), Hong Kong in 2010. He is currently working toward the M.S. and Ph.D. degrees in electrical engineering at Stanford University, Stanford, CA, USA.

He is a National Defense Science and Engineering Graduate (NDSEG) Fellow at Stanford University.



Sanghoek Kim (Student Member, IEEE) received the B.S. degree with a double major in electrical engineering and mathematics from Seoul National University, Seoul, Korea, in 2007 and the M.S. degree in electrical engineering from Stanford University, Stanford, CA, USA, in 2009, where he is currently working toward the Ph.D. degree.

His research interests include wireless power transfer and biomedical applications of radio-frequency technology.

Mr. Kim is a recipient of the Kwanjeong Educational Foundation Scholarship.



Ada S. Y. Poon (Senior Member, IEEE) was born in Hong Kong. She received the B.Eng. and M.Phil. degrees in electrical and electronic engineering from the University of Hong Kong, Hong Kong, in 1996 and 1999, respectively, and the M.S. and Ph.D. degrees in electrical engineering and computer sciences from the University of California at Berkeley, Berkeley, CA, USA, in 1999 and 2004, respectively.

In 2004, she was a Senior Research Scientist at Intel Corporation, Santa Clara, CA, USA. In 2005, she was a Senior Technical Fellow at SiBeam, Inc., Fremont, CA, USA. In 2006–2007, she was an Assistant Professor at the Department of Electrical and Computer Engineering, University of Illinois at Urbana-Champaign, Urbana, IL, USA. Since 2008, she has been at the Department of Electrical Engineering, Stanford University, Stanford, CA, USA, where she is currently an Assistant Professor. Her research focuses on applications of wireless communication and integrated circuit technologies to biomedicine and healthcare.

